Hybrid numerical-experimental study of an offshore piezoelectric energy harvesting from water waves

Seyed Behnam Hosseini
Mohammad Mostafa Mohammadi *Jafar Ghazanfarian*[*]

Mechanical Engineering Department, Faculty of Engineering, University of Zanjan, Zanjan, Iran,
Tel.: +98 (24) 33054142, +98 9121417283, P.O. Box 45195-313.

Abstract

A novel cantilever piezoelectric energy harvester with a modified structure of tilting beam has been designed to harness energy from water waves. New suggestions are presented for analysis of the interaction of the nonlinear waves with the beam surface using a hybrid theoretical/experimental approach. The experimental tests are conducted to investigate the effect of different design parameters such as the longitudinal distance of the cantilever beam from the wave-maker, the shape of the oar-like tip of the beam, the angle of spatial orientation, the strength of the waves, the material of piezo-harvester, and the depth of the beam below the free-surface on the output voltage. Numerical simulations are conducted based on the beam deformation captured by a high-speed camera. It is found that adding the torsional moment led to the generation of about 13% and 50% higher root-mean-square and peak-to-peak voltages in comparison to the pure-bending case, respectively. By increasing the indentation from 3 cm to 6 cm, about an 18% increase can be captured in produced voltage. These results can be used to train a model for a control system to keep the optimum angle between the water waves and the beam.

Keywords: Water waves, energy harvesting, piezoelectric effects, free-surface flows, direct energy conversion

Nomenclature

D_i	electric displacement
E_b	Young's modulus of steel beam
E_i	electric field
E_p	Young's modulus of piezoelectric layer
F_i	force
g	thickness of piezoelectric layer
h_b	thickness of piezoelectric beam
h_p	thickness of piezoelectric layer
h_1	the harvester depth
h_2	the wave maker depth
L	length
S_{ij}	strain tensor
t	time
T_{ij}	stress tensor
u	displacement
v_i	velocity
V_{rms}	RMS voltage
V_{pp}	pick-to-pick voltage
Greek letters	
ϵ	dielectric permitivity
ρ_b	density of beam
ρ_p	density of piezoelectric layer
ψ	electric potential

1 Introduction

With explosively increasing demand for self-powered systems, such as low-power electronic devices, wireless communication systems, and electronic sensors, the energy harnessing by converting the mechanical energy of the ambient vibration into the electrical energy and hybrid all-in-one package harvesters [1] have turned out to be an open research field [2]. The level of generated energy is a challenging and complex issue in studying energy harvesters used in various real-world applications.

Ghazanfarian et al. [2] presented and classified various reviews written about piezoelectric harvesters, putting special emphasis on the energy output of such devices. Kargar and Hao [3] presented an atlas of piezoelectric energy harvesters in oceanic applications. They indicated that among all the developed harvesters, piezoelectric energy harvesters suggest the most promise for omitting batteries from devices. The reason is that piezo devices are maintenanceless and compact with simple structures. They can be attached to low-power devices to generate high-density power directly.

Due to the power of moving water waves [4, 5, 6] to induce vibration, harvesting the mechanical energy from surface waves in sea, ocean, and river has long been pursued as an alternative self-containing energy source [7]. In addition,

the piezoelectric harvesters are the most promising devices to eliminate batteries [8]. Ertutk and Inman [9] compared the power density as a function of output voltage generated by fuel cells, solar cells, thermoelectric, electromagnetic, and piezoelectric harvesters. However, there are partial overlaps between different fields, and a wider area can be covered by piezoelectric harvesting devices.

For instance, an expedient piezoelectric coupled buoy energy harvester has been developed from ocean waves [10, 11]. Their new harvester comprised several piezoelectric coupled cantilevers attached to a floating buoy structure, which could be easily suspended in the intermediate and deep ocean. They investigated the effect of dimensional parameters of the designed structure on the output voltage using finite element simulations.

Oy [12] performed an experimental energy generation procedure for small-scale applications. A new circuit topology and 20 diaphragm-type PZTs on a mass-spring structure have been introduced to increase the generated power. Mariello et al. [13] designed a hybrid piezo/triboelectric hybrid water nanogenerator. Their device is a multifunctional, flexible, conformal harvester with a sub-100μm thickness and biocompatible thin-film piezo-ceramic.

Formation of water waves [14] due to oscillation of bodies or fluid-structure interaction can be a source of energy. Dai et al. [15] investigated piezoelectric energy harvesting from concurrent vortex-induced vibrations and base excitations. The harvester consists of a multi-layered piezoelectric cantilever beam with a circular cylinder tip mass attached to its free end. It is placed in a uniform air flow and subjected to direct harmonic excitations. Molino-Minero et al. [16] investigated the energy generated from the piezoelectric materials due to induced water flow vortices. The vortices were generated by cylinders of different sizes attached to a piezoelectric cantilever beam. They evaluated the performance of the system for different cylinder diameters.

Lee et al. [17] fabricated a piezoelectric flow energy harvesting device containing a cantilevered transducer with one or several piezoelectric material layers attached to the surface. They used this harvester to empower some small-scale systems. The experimental results demonstrated that the constructed harvester produced 20 mW power with a flow rate of 20 L/min and a pressure drop of 165 kPa.

Bahmanziari and Zamani [18] proposed a fractional-order PID controller based on combining magnetic plucking (MP), mechanical impact (MI), and mechanical vibration force (MVF) to improve electrical energy harvesting from piezoelectric smart tiles. They determined the proper air gap between the console and the stopper and captured an average power of 71.0 mJ and 13.6 mW in the optimal resistance case.

Burns et al. [19] mechanically coupled a floating body on the water to a piezoelectric setup. Upward and downward movement of the float in the water induced vibrations on the piezoelectric material, leading to the generation of output power. They declared that to increase the energy transfer efficiency, the output impedance of the float was matched with the input impedance of the piezoelectric members. Kazemi et al. experimentally investigated energy harvesting from longitudinal and transverse water waves using a piezoelectric

device. They also proposed the optimum electrical load resistance to harvest maximum power. It is found that the maximum density of the harvested electrical power from a waterproof piezoelectric wave energy harvester was increased compared to the other similar works[20].

Song et al. [21] constructed a novel piezoelectric energy harvester with two piezoelectric beams and two cylinders. The energy harvester could convert the kinetic energy of water into electrical energy employing vortex-induced vibration (VIV) and wake-induced vibration (WIV). They found that the vibration of the upstream cylinder was VIV-type, which enhances the energy harvesting capacity of the upstream piezoelectric beam. For the downstream cylinder, both VIV and WIV types could be obtained. They found that the downstream beam achieves a better energy harvesting performance with increased water velocity.

Sui et al. [22] proposed a magnetically coupled piezoelectric energy harvester for efficient energy harvesting in low-velocity water environments. They evaluated the effects of the diameter and mass of the vibrating column, the vertical distance between magnets in their structure, and the flow velocity on the output performance of the piezoelectric harvester.

Hassan et al. [23] simulated a piezoelectric transducer that could harvest energy from a fluid stream. The vortex shedding and the varying lift forces resulted in fluctuating the fluidic pressure impulse on the beam. They caused the flexible cantilever beam to oscillate in the direction normal to the fluid flow in a periodic manner. In this work, the material properties and design of the harvester are kept unchanged, whereas the simulations were performed with different fluids and varying flow characteristics. To optimize the output electrical energy, the size and geometry of the obstructing entity were systematically varied. Allen et al. [24] fabricated an energy-harvesting eel using flexible piezoelectric membranes. The membranes were excited by the von Karman vortex street forming behind a bluff body. They examined the response of the flexible membrane or the eel to external forcing due to the vortex shedding in the wake.

Mujtaba et al. [25] recently proposed a two-piezoelectric tandem flag arrangement under the influence of the wake of an upstream bluff body. They placed the flags behind the bluff body and investigated the flapping behavior. Their results showed that the flapping amplitude of the rear flag is increased by excitation from the vortices and wake of the front flag, which enhances the energy harvester efficiency based on the flapping frequency and the random excitations with high amplitudes.

Shan et al. [26] investigated the harvested energy of a piezoelectric cantilever beam with twisting and bending oscillations in the stream of low-speed water flow. Song et al. [27] performed numerical and experimental studies on harvesting energy from vortex-induced cylinder vibrations in flowing water. The effect of the electrical load resistance, the water velocity, the cylinder mass, and the diameter have been numerically and experimentally analyzed. Latif et al. [28] analyzed the effect of wake fluctuation on the performance of a piezoelectric energy harvester positioned behind two circular cylinders along the wave symmetry line. They remarked that employing two cylinders in a side-by-side configuration results in a significant increase in the output power of the har-

vesters.

Shan et al. [29] made a macro fiber composite piezoelectric energy harvester, which was submerged into the water vortex shedding from an upstream cylinder. In this work, the energy harvesting ability of the piezoelectric harvester was numerically and experimentally investigated versus the flow velocities and the diameter of the cylinder. They analyzed the output power of the piezoelectric energy harvester with respect to the cylinder diameter and the water velocity.

Karimzadeh et al. [30] numerically simulated a cylinder-based harvesting device from the wind. They modeled the imposed lift force and used the numerical tool to solve the coupled governing equations of deflection, electrical part, and fluid flow. Hu et al. [31] designed a galloping piezoelectric energy harvester to harness the energy from low-velocity water flow. Their energy harvester includes two bluff bodies in an elliptical cylinder shape, and they investigated the effect of surface roughness of bluff bodies on the performance of the energy harvester.

Li et al. [32] demonstrated the energy harvesting from low-frequency sonic waves in a square channel. Their acoustic energy harvester contained a quarter-wavelength straight tube resonator with lead zirconate titanate (PZT) piezoelectric cantilever plates placed inside the tube. In order to increase the output voltage power, multiple PZT plates were employed. They found that it is more beneficial to place the piezoelectric plates in the first half of the tube rather than along the entire tube.

Zhang et al. [33] utilized the non-linear magnetic forces to enhance energy harvesting in piezoelectric energy generators. Their energy harvester showed a softening behavior in the bistable region due to the introduced nonlinear magnetic force. Also, their results indicated that the output power of the energy harvester had been increased up to 29% with respect to the conventional configuration.

Weinstein et al. [34] made a cantilevered piezoelectric beam and exposed it to a heating, ventilation, and air conditioning (HVAC) flow. The excitation of the beam was amplified by enhancing the interactions between an aerodynamic fin at the end of the piezoelectric cantilever and the vortex shedding downstream of the bluff body placed in the airflow ahead of the aerodynamic fin. They achieved the maximum power output when the shedding frequency matched the beam resonance frequency. They tuned the resonance frequency of the piezoelectric harvester by positioning small weights along the fin.

Belkourchia et al. [35] successfully modeled the energy scavenging from fluid-structure interaction by combining the finite element method with the quadratic differential method. They employed the Navier-Stokes equation for the fluid flow and the Euler-Bernoulli beam theory for the cantilever structure. Yamac et al. [36] utilized the fluid dynamics software FLUENT to numerically model water waves created in a water channel by a wave-maker. They employed the dynamic-mesh technique and the volume of fluid method in their model. They analyzed the buckling of the harvester plate using the transient structural module and calculated the generated power from the root mean square (rms) equation. Also, they investigated the effect of the underwater position of the wave harvester, the water depth, the wave amplitude, and the period on the amount of the

produced electrical energy.

Adabzadeh et al. [37] presented the piezoelectric energy harvester of cantilever type with the ability to be angled relative to the vertical direction, and also with rectangular fins attached to the end of the harvester. The experiments have been designed using the central composite design (CCD) and experimental model analysis and design parameters have been optimized using the response surface methodology (RSM). The main purpose of the study was to investigate the effect of design parameters such as the angle of inclination of the energy harvester, its distance from the wave source, the depth of the beam, and the presence or absence of fins at the end of the beam, on the effective voltage of the energy harvester output. Rajabi et al. [38] presented a purely numerical, fully-coupled-fluid-structure-piezoelectric model based on the finite-element method. They found that attaching mass to the tip of the beam leads to a 13.5% rise in the output voltage compared to the state without the attached mass. They investigated the influence of the load resistance on voltage and the output power. It is seen that the power has an optimum load resistance that is 2.61 times higher than the reference state.

A novel piezoelectric energy-harvesting structure with different oar-like fins attached to the tip of a cantilever beam has been proposed to harness energy from water waves. There is a research gap in implementing a hybrid optical-numerical study. Due to the chaotic nature of such problems, pure numerical methods may have large errors or numerical noises. Using such hybrid techniques, we can obtain more accurate results. To the best of our knowledge, the present paper is the first study that combines the power of optical method with the flexibility of numerical techniques.

The contributions and the novelties of the present paper are as follows.

- Investigation of the voltage output from water waves for tilting structures with different geometries using an optical-numerical approach is a new field of research, which can pave the road for optimization studies, machine learning-based modelings, and design of control systems for harvesters with varying beam angles.

- Effects of new design parameters such as geometric variables, shapes of the oar and obstacle, spatial and angular positions of the beam in the channel on the output voltage of the harvester have been investigated using experimental approach.

- Orientation of the beam with respect to the free-surface water waves, effects of sharp edges of the obstacle on flow pattern, and the virtual mass of the added tip have been discussed to harvest energy with higher efficiency.

- A hybrid optical-numerical technique was used to calculate the output voltage of the harvester using a high-speed camera to evaluate the generated voltage of different piezo-materials, including barium titanate, cadmium sulfide, PZT-5H, and PZT-4.

The rest of the paper is organized as follows. Section 2 illustrates details of the experimental setup. In Sec. 4 details of the numerical simulations have been presented. After validation of the results, physical discussions and concluding remarks have been indicated in Secs. 3 and 5, respectively.

2 Experimental setup

As shown in Fig. 1, our experimental setup consists of a water channel equipped with a wave-maker, a piezoelectric cantilever beam, an obstacle insert, the piezomaterial, the electrical circuitry, a digital oscilloscope to measure the output voltage, and a high-speed camera with the frame rate of 100 frame/sec. The piezoelectric harvester is attached near the base of the fixture. The tip of the beam is submerged under the free-surface of water in the channel. The output voltage of the piezoelectric harvester was measured and plotted by a digital oscilloscope.

The water channel is made of transparent Plexiglas with 7.3 m length, 0.6 m width, and 0.6 m height. The wave-maker has two rectangular fins rotating in water using an electrical motor. A screw is used to adjust the depth of penetration of the wave-maker in the water to generate waves with different heights. The piezoelectric material is the PZT(5H) ceramic disc attached near the base of a rectangular stainless-steel beam. The physical properties and other geometrical details of the experimental setup, such as the piezomaterial, the beam density, Young's modulus of the beam, the piezomaterial, the beam thicknesses, the length and breadth of the beam, are listed in Table 1.

Table 2 presents the range of variation of parameters in experiments, including the penetration depth of the beam and the wave-maker, the longitudinal distance between the wave-maker and the beam, the shapes of the oar and the obstacle, and the beam angle. The rotational speed of the wave-maker is 53 rounds per minute. The peak-to-peak voltage and the root-mean-square (RMS) voltage of the harvester were measured as the output parameters of the piezoelectric harvester. The RMS voltage was measured directly by a digital oscilloscope. The commercial code of the oscilloscope was GPS Limited 1072B+. The range of change of each parameter is determined based on a set of initial experiments. The strategy of experimentation is the one-factor-at-a-time (OFAT) approach. The OFAT method is performed by selecting a starting point, or a baseline set of levels for each factor, and then successively varying each factor over its range with other factors held constant at the baseline level [34].

It is also necessary to check the effect of refraction on measured deformations before conducting experiments. The optical measurement setup has been calibrated by comparing the captured displacement of the beam in air and water.

Each experimental run has been repeated at least three times, and the average value of the outputs has been reported. The standard deviation was calculated using Equation 1:

$$\sigma = \sqrt{\frac{\sum_{n=1}^{N} \bar{x} - x_i}{N-1}} \tag{1}$$

where $\bar{x}$ and x_i are the average value and the result of each experiment, respectively. The uncertainty of the average value of experiments has been evaluated by dividing the standard deviation of the experiments by $\sqrt{N}$. Here N is the number of repeated measurements. By dividing the uncertainty of the average value by the mean value, the fractional uncertainty can be evaluated in percent [39]. The evaluated fractional uncertainty of the experiments for the peak-to-peak voltage and the RMS voltage were 11% and 4%, respectively.

3 Results and discussion

3.1 The streamwise distance

The effect of the longitudinal distance of the piezoelectric harvester from the wave-maker is evaluated, keeping other parameters unchanged. The beam is a simple rectangle without an ore-shaped end. The results are helpful in determining the best installation location of the harvester relative to the source of the waves. The penetration depth of the harvester and the wave-maker blades under the water free-surface is 4.5 cm, the angle of the piezoelectric harvester with respect to the vertical direction is zero, and the longitudinal distance (L) varies from 40 cm to 100 cm. The experiments are repeated five times for all cases. The peak-to-peak voltage and RMS voltage are measured using a digital oscilloscope.

Figure 2 represents the variation of the peak-to-peak and the RMS voltage of the harvester versus the longitudinal distance from the wave-maker. It can be concluded from the figure that as the longitudinal distance decreases from 100 cm to 40 cm, the RMS and the peak-to-peak (PP) voltages increase by about 110% and 200%, respectively. Such trends in the output energy as a function of distance from the source of generation of the wave originate from enhanced deformation of the beam due to the higher hydrodynamic loads of the waves.

3.2 The tilt angle

Variation of the output voltage versus different cantilever beam angles measured from the vertical direction has been investigated using the experimental setup. In this case, the longitudinal distance of the rectangular beam from the wave-maker is fixed at 60 cm, and the beam penetration length is 3, 4.5, and 6 cm. The tilt angle is changed from -15° to 40°, and the peak-to-peak and the RMS voltages were measured and plotted in Fig. 3. The beam was a simple rectangle without any ore end. It should be noted that the positive title angle indicates the inclination of the beam toward the upstream flow.

It is found that by increasing the tilt angle from negative values up to positive angles, the peak-to-peak and the root-mean-square voltages continuously experience up to 90% and 70% increase, respectively. This trend has two origins. The first one is the streamwise deflection of the beam, which is in contrast to the positive tilt angles and intensifies the deflection of the beam. In reverse, when the beam is initially titled to the left for negative tilt angles, the output

voltage reduces. The second reason for such growth in the output power when the beam is highly titled to the right is the pattern of the free-surface near the tip of the beam. As shown in Fig. 4 a-b at such an inclined configuration, the beam temporarily gets out of the water, and the exerted hydrodynamic force vanishes. This phenomenon empowers the dynamic behavior of the load on the beam and enhances the output voltage.

The other point in Fig. 3 is the effect of the penetration depth of the tip of the beam in the water on the output voltage. It is seen that the effect of the penetration depth is more pronounced when the tilt angle is non-zero, and the harvester is not vertically oriented. So, it is recommended to increase the depth of penetration of the tip, precisely when the beam is tilted. Changing the penetration depth from 4.5 cm to 6 cm leads to an increase of about 50 % in the output voltage in the off-vertical position. In fact, by increasing the penetration depth, the projected frontal area and the wetted area of the beam below the free-surface become more prominent, which enhances the mechanical deflection of the piezoelectric cantilever and the produced voltage.

A deep analysis of the flow pattern proved that the output voltage is directly related to the angle of collision of the free-surface with the beam, which is also a function of the tilt angle of the harvester. To visualize this trend, the impact angle between the water surface wave and the beam in different spatial configurations has been calculated using the flow snapshots. The results at two instants of time belonging to each case are illustrated in Fig. 4c-f for the penetration length of 4.5 cm. It is found that by decreasing the tilt angle from 40° to -15°, the impact angle between the wave and the beam decreases from 95° to 52°. Another point here is the effect of the penetration depth and the inclination angle on the distance of the beam from the wave maker. When the inclination angle or the penetration depth increase, automatically the distance between the beam and the energy source reduces. This may be another reason for a higher voltage output obtained in figures.

It is concluded that a collision angle close to 90° leads to more robust energy transmission, and as a result, the output voltage grows. In other words, the right impact angle generates higher normal component of the applied hydrodynamic load compared to the tangential component. Consequently, a larger deflection in the beam appears. It is also found that the impact angle for cases with 0° and 15° tilt angle is higher for 3 cm indentation (75° and 79°, respectively) in comparison to 4.5 cm penetration case (64° and 78°, respectively). This trend leads to an increase in the output voltage for the mentioned cases in Fig. 4.

3.3 The shape of the oar

The hydrodynamic loading on the piezoelectric cantilever beam depends on the shape of the tip of the steel beam. To investigate the influence of the shape of the oar-like beam, four different geometries are shown in Fig. 5. The connecting point of each oar-like appendix to the beam equals 2 cm measured from the tip edge and is the same for all cases. The length and the width of all cross sections are 12 cm and 5 cm, respectively, except for the square case,

which has the same side lengths. It is shown that three attaching configurations have been considered for the rectangular oar-like insert to visualize the effect of the torsional and the bending moments as well as the form drag force.

During the experiments of the present case, the wave-maker penetration depth is fixed at 4.5 cm, the beam penetration is 2.5 cm, the tilt angle of the steel beam is zero, and the longitudinal distance of the piezoelectric harvester from the wave-maker is 60 cm. Each oar shape has a different area based on its geometry. Figure 6 illustrates the variation of the output RMS voltage and the peak-to-peak voltage having the oar-end area as the abscissa of the graph.

The distance of the piezomaterial from the neutral fiber and the moment of inertia around the neutral axis are similar for all cases. Based on the relation $F_D = \frac{1}{2} C_D \rho A V^2$ where C_D , ρ, A and V are the drag coefficient, the water density, the projected area, and the water wave velocity the most influential parameters are the drag coefficient of the beam and the area of the oar appendix. Due to the transient nature of oscillations, the other effectual quantity is the virtual mass of the system. As a result, we have captured two contradictory behaviors in the case of an oscillating oar-like harvester inside water.

The rectangle case ($A = 60cm^2$) mentioned inside Figs. 6 a and b correspond to the case d in Fig. 5. The results presented for cases a and b in Fig. 6 indicate that as the frontal area and the drag coefficient increase (the viscous effect) due to the non-aerodynamic shape of the oar, simultaneously, the magnitude of the added mass coefficient (inviscid effect) grows as well. Consequently, a larger volume of the surrounding water should be accelerated or decelerated. Hence, we have a decreasing trend in the output voltage from the square oar to the rectangular cross-section. It should be emphasized that the added mass concept can be neglected for air due to its small density. Accordingly, this trend is expected to be reversed for the harvesters operating in gases with a small influence of the added mass.

The output RMS and the peak-to-peak voltages of the concentric horizontal (case d), the out-of-center horizontal (case e), and the vertical rectangular oars (case f) have been compared in Fig. 6c,d. The added mass for these cases can be assumed to be approximately the same. The results proved that the output RMS and the peak-to-peak voltages for the concentric horizontal rectangle (case e) are greater than the vertical case (case f) due to higher exerted form drag force. However, adding the torsional moment in case e has resulted in about 13% and 50% increase in the RMS and the peak-to-peak voltages, respectively, with respect to the pure-bending output (case d). The increase in the output voltage by adding the torsional moment is in accordance with the data reported by Shan [26].

The torsional loads create shear stresses (like T_{13} stress component) on the piezoelectric layer and upon equation $D_i = e_{ijk} T_{jk} + \epsilon_{ij} E_j$, these shear stresses are multiplied by the piezoelectric coefficients and result in the creation of electric displacement and electric voltage in the piezoelectric material. A complete mathematical analysis of the problem may be found in [26]. In Ref. [26], it was shown that the torsional loads can enhance the output power of the harvesters by nearly 99 percent.

3.4 The wave power

Increasing the wave-maker penetration depth under the water free-surface leads to generating high-energy containing waves with higher heights. In the experiments designed for this section, the common configuration has been selected for the beam, the longitudinal distance of the piezoelectric harvester from the wave-maker is 100 cm, the penetration depth of the harvester is 4.5 cm, and the harvester had zero tilt angle with respect to the vertical axis. The wave height in Fig. 7 can be measured based on the maximum elevation of the fluid particle located on top of the wave. It should be noted that since the wave height continuously changes with time, different wave heights have been created by changing the penetration depth of the wave-maker blades.

Figure 7 illustrates the maximum wave heights measured for different penetration depths of the wave-maker. It is seen that the amplitude of the wave decreases from about 8.7 cm to 6.2 cm by decreasing the penetration depth of the wave-maker. Figure 8 shows the variation of the effective and the peak-to-peak voltages of the harvester as a function of the penetration depth of the wave-maker. As presented in the figure, by about a 40% increase in the wave height, the effective voltage experiences an increase from 0.64 V to 0.80 V (25 %), and the peak-to-peak voltage increases from 4.2 V to 5.25 V (25 %).

3.5 The shape of the obstacle

Two cylindrical obstacles with circular cross-section and equilateral triangular shell have been examined. Figure 1 demonstrates a schematic view of the test configuration, including an obstacle. The outer diameter and the height of the circular obstacles are 6 cm and 20 cm, respectively. The equilateral cylindrical shell has a 5 cm leg length and 20 cm height. In experiments of the present section, the longitudinal distance of the wave-maker from the piezoelectric harvester is 70 cm, the penetration depth of the harvester is 2.5 cm, and the beam is vertical. The shape of the steel beam has been indicated in figure 1, and the longitudinal distance of the obstacles from the piezoelectric harvester (L) is different for each experiments.

The presence of an obstacle against a stream has two different effects. Positively, it may change the frequency of induced vibrations and cause resonance due to turbulence promotion. This trend may increase the output voltage. On the other hand, the obstacle may act as a block against the incoming fluid, and damps the wave power, which leads to the reduction of incoming momentum exchange with the beam. In our case, we face the blockage effect of the obstacle, as is evident from the name "obstacle". We tried to compute the effect of inserting the beam at different distances from an unwanted obstacle (like natural bumps or artificial human-made obstructions) on the output. Values of the peak-to-peak and the RMS voltages for the case without obstacles are 6.4 V and 1.12 V, respectively.

Figure 9 illustrates the variation of the peak-to-peak and the RMS voltages of the piezoelectric harvester as functions of the distance L. As shown in

Fig. 9, the cylindrical obstacle is more effective in increasing the output voltage than the equilateral shell. Also, the maximum voltage of about 0.96 V is achieved when the longitudinal distance is 30 cm. For the equilateral obstacle, the maximum voltage occurs when the obstacle is positioned 20 cm away from the energy harvester. Unlike the cylindrical obstacle, the output voltage decreases by increasing L for this type of obstacle.

It is seen that the influence of the shape of the obstacle on Karman's vortex street is similar when the distance is about 20 cm. However, the output power grows for the cylindrical obstacle by increasing the distance downstream of the obstacle. So, the optimum dimensionless distance to insert the harvester behind a circular obstacle using the radius of the obstacle as the length scale is 5. By increasing the beam-to-obstacle distance, the dynamic nature of the vortical flow inside the wake region damps out, and the voltage reduces in both cases.

4 Numerical-optical modeling

Piezoelectric materials produce the output voltage when subjected to mechanical deformation. Here, we write the governing equations of piezoelectricity in strain-charge format. The electric field components can be related to the electric potentials using the electric potential (ψ) concept, and the electrical displacement field is divergence-free based on Maxwell's relations

$$E_i = -\psi_{,i}, \quad D_{i,i} = 0 \tag{2}$$

The electrical and mechanical constitutive relations read

$$D_i = d_{ijk}T_{jk} + \epsilon^T_{ij}E_j \tag{3}$$

$$S_{ij} = S^E_{ijkl}T_{kl} + d_{kij}E_k \tag{4}$$

where S_{ij} is the strain tensor, S^E_{ijkl} is the compliance tensor, T_{jk} is the mechanical stress tensor, D_i represents the electric displacement, E_k is the electric field, d_{ijk} is the piezoelectric coefficient, and ϵ^T_{ij} is the dielectric permittivity tensor. In our numerical study, the steel beam is supposed to be a linear elastic material with small displacements. Navier's equation for the mechanical equilibrium, along with the strain-stress relation, is

$$T_{ij,j} + F_i = \rho\frac{\partial^2 u_i}{\partial t^2}, \quad S_{ij} = \frac{1}{2}(u_{i,j} + u_{j,i}) \tag{5}$$

where F_i, u_j are the body force and the displacement, respectively. For a PZT ceramic, Equations 3 may be written in matrix form as

$$\begin{pmatrix} D_1 \\ D_2 \\ D_3 \end{pmatrix} = \begin{pmatrix} 0 & 0 & 0 & 0 & d_{15} & 0 \\ 0 & 0 & 0 & d_{24} & 0 & 0 \\ d_{31} & d_{32} & d_{33} & 0 & 0 & 0 \end{pmatrix} \begin{pmatrix} T_1 \\ T_2 \\ T_3 \\ T_4 \\ T_5 \\ T_6 \end{pmatrix}$$

$$
+ \begin{pmatrix} \epsilon_{11} & 0 & 0 \\ 0 & \epsilon_{22} & 0 \\ 0 & 0 & \epsilon_{33} \end{pmatrix} \begin{pmatrix} E_1 \\ E_2 \\ E_3 \end{pmatrix}
$$

$$
\begin{pmatrix} S_1 \\ S_2 \\ S_3 \\ S_4 \\ S_5 \\ S_6 \end{pmatrix} = \begin{pmatrix} s_{11} & s_{12} & s_{13} & 0 & 0 & 0 \\ s_{21} & s_{22} & s_{23} & 0 & 0 & 0 \\ s_{31} & s_{32} & s_{33} & 0 & 0 & 0 \\ 0 & 0 & 0 & s_{44} & 0 & 0 \\ 0 & 0 & 0 & 0 & s_{55} & 0 \\ 0 & 0 & 0 & 0 & 0 & s_{66} \end{pmatrix} \begin{pmatrix} T_1 \\ T_2 \\ T_3 \\ T_4 \\ T_5 \\ T_6 \end{pmatrix}
$$

$$
+ \begin{pmatrix} 0 & 0 & d_{13} \\ 0 & 0 & d_{23} \\ 0 & 0 & d_{33} \\ 0 & d_{42} & 0 \\ d_{51} & 0 & 0 \\ 0 & 0 & 0 \end{pmatrix} \begin{pmatrix} E_1 \\ E_2 \\ E_3 \end{pmatrix} \tag{6}
$$

Kundu et al. [40] presented the output power at various frequencies for a vibrating beam with an added mass attached to the end of the beam. They obtained results using analytical and numerical methods. We compared the results of our numerical technique with those of Kundu et al. [40] in Fig. 10 for 10 $k\Omega$ and 100 $k\Omega$. It is found that with a good accuracy, at the resistance of 10 $k\Omega$, the output power reaches 0.33 mV with the resistance of 10 $k\Omega$.

The piezoelectric energy harvester used in our experiments is made of PZT(5H) ceramic disc and is attached to a rectangular stainless-steel beam near the root of the beam. By deflecting the beam via the pushing momentum of the water waves, the piezoelectric disc also deflects, and consequently is polarized. The root of the harvester is fixed and its tip penetrates in the water, exposing to the stream of waves. By supposing a rigid attachment of the PZT disc to the steel beam, the displacement components, and the strain field over the contact area were obtained, and the electric displacement and the electric potential were computed.

Deformation of the free vibrating tip of the harvester under the effect of the water flow has been captured by a high-speed optical camera. Then, the deformation of the beam during vibrations has been imported to the finite element algorithm as the instantaneous displacement of the tip of the beam at each time-step. The optical measurement system was calibrated with a predetermined deformation in the water. Using this hybrid numerical-experimental strategy, the deformation of the beam was captured in experiments and the output voltage was calculated both from the numerical simulations and as the output signal of the oscilloscope. The hybrid nature of the numerical method helps us omit complexities of the flow field as well as uncertainties stemming from turbulence, transients, the motion of blades of the wave-maker, and nonlinearities of the fluid motion. Based on the time-step size independence study, the value of the time-step size should be 0.015 s.

Figure 11 compares the optical visualization of the beam deflection in water and the corresponding computed beam deflection based on simulations. The displacement of the beam tip has been extracted from snapshots of the flow field to be 13.59 mm, 2.85 mm, and 22.48 mm at 0.9984 s, 5.1168 s, and 49.795 s, respectively. The deflections of the beam obtained from the experimental data agree with the results of the hybrid numerical-optical simulations. The important point about this figure is the refraction of the light near the free-surface during optical photo capturing which may be a source of error.

Two-dimensional square elements have been selected in Fig. 12 to discretize the geometry. The mesh-independence analysis was performed based on the variation of the RMS voltage produced by the PZT disc for the constant displacement regime. Figure 12 demonstrates the results of the convergence analysis based on the variation of the output RMS voltage of the harvester. The details of the computational grid used to discretized the beam and the piezoelectric material placed on it is presented in the insert of the figure. As shown in Fig. 12 the fifth mesh topology is fine enough to be selected as the best choice to generate convergent results. The mesh number 1 to 6 in the figure includes 814, 1374, 2380, 3164, 4730, and 5418 number of nodes in the piezomaterial, and 3124, 5376, 9428, 12582, 18886, 21654 mesh points inside the beam.

Figure 13a illustrates the measured and simulated temporal variation of the output voltage of the piezoelectric energy harvester. The hybrid numerical-experimental and the pure experimental results for the RMS voltage, the average voltage, and the peak-to-peak voltage are also presented in the legend of the figure. The relative errors of simulated results for the RMS, the average, and the peak-to-peak voltages compared to the measurements are 29%, 11%, and 37%, respectively. In addition, the Fourier transform of temporal variation of the experimental and numerical data related to the voltage output is presented in Fig. 13b. It is seen that most of the hidden dominant frequencies can be captured by the numerical model. The chaotic nature of the flow-beam configuration is the origin of such scattered distribution of frequencies. The FFT analysis helps up capture the most dominant frequencies.

Figure 14 presents the output voltage of point B in Fig. 2, obtained from the numerical modeling using four different piezomaterials, including barium titanate, cadmium sulfide, PZT-5H, and PZT-4. The effective output voltage for each case equals 0.223 V, 0.018 V, 0.053 V, and 0.045 V, respectively. The highest instantaneous voltage about 0.7 V, belongs to barium titanate. The highest voltage is a critical point in the design of circuitry. The electrical circuit should tolerate the generated peak voltage. However, the output power is proportional to the RMS voltage. So, the ratio of the RMS voltage and the maximum voltage may be a design parameter, which approximately equals 0.32, 0.30, 0.27, and 0.38 for the mentioned materials, respectively.

In order to analyze the effect of the material properties a sinusoidal load of $500\sin(5\pi t)$ was applied to the end of the beam, and the resulting mechanical stress component T_{11} and the electric displacement on the piezoelectric disc have been simulated. The resulting stresses on barium titanate and PZT 5H are shown in Fig. 15.

As shown in the figure, the loading has resulted in a bigger stress component T_{11} in barium titanate with respect to PZT. On the other hand, the output open-circuit voltage of the piezoelectric layer may be calculated by [41]:

$$v = \frac{d_{ij}}{\epsilon_r \epsilon_0} \sigma_{ij} g_e \tag{7}$$

where d_{ij}, σ_{ij}, ϵ_r, ϵ_0, and g_e are the piezoelectric coefficients, the stress tensor, the dielectric coefficient, the vacuum permittivity and the inter-electrode gap (here thickness of the piezoelectric layer). Accordingly, the enhancement of the mechanical stresses, the piezoelectric coefficients, and the reduction of the dielectric coefficients result in an increase of the electric voltage. In our problem, the main stress component is T_{11}, and the coupling mode of the cantilever is the 31 mode. The main piezoelectric coefficient is d13. This coefficient equals -3.45×10^{-11} C/N for barium titanate and -2.74×10^{-10} C/N for PZT(5H). Also, the dielectric coefficients of $BaTiO_3$ are smaller than similar to those of PZT (5H). Thus, $BaTiO_3$ generates higher electric voltages.

In order to numerically simulate the effect of the wave force on the beam deformation, we have optically measured the time-dependent wave-induced displacement of the beam. The data have been imported to the numerical part as a boundary load. Using this hybrid optical-numerical technique, the direct simulation of the wave force can be ignored. However, we need to independently compute the deformation of the beam using the numerical code. This point can be the topic of future works. Simulation of the wave formation process and its interaction with the beam are sophisticated due to the chaotic nature, turbulence, three-dimensionality, fluid-structure interaction, free-surface deformation, and multi-physics nature. The numerical part was used to investigate the effect of material properties and to obtain data to compare with the experimental results. Also, if we train the data in the present paper, we can construct deep learning models based on reinforcement learning concepts.

5 Conclusion

Energy harvesting from water waves via an oar-shaped piezoelectric cantilever beam has been experimentally and numerically studied. The effect of the piezoelectric harvester penetration depth, the wave-maker penetration depth, the shape of the oar-like tip of the beam, the beam angle, and the shape of the obstacle placed in front of the piezoelectric harvester on the output voltage of the harvester was investigated. We used the one-factor-at-a-time (OFAT) approach as the strategy of experimentation.

In order to numerically simulate the output of the piezoelectric energy harvester, the water-wave-induced tip movements of the steel beam were measured during the harvesting period and fed into the model as a boundary condition. Using this technique, the need to simulate the coupled complicated hydro-mechanical interactions can be omitted. The optimization of the piezoelectric energy harvester and fabrication of hybrid harvesters are our future

research recommendations. The following advice was concluded based on the experiments.

1. Increasing the piezoelectric harvester penetration depth results in the enhancement of the output voltage of the harvester. This is due to the increment of the contact area of the steel beam with the water wave. It is calculated that changing the penetration length from 4.5 cm to 6 cm leads to an increase of about 50 % in the output voltage in the off-vertical position.

2. The tilt angle of the piezoelectric harvester was another effective parameter of the experiments. Increasing the tilt angle from -15 to 40 degrees leads to the variation of the impact angle between the wave and the beam in the range of 51.43° to 96.16°. For a constant penetration depth, approaching the wave impact angle of 90° resulted in an increase of the normal component of the applied hydrodynamic load, in comparison to the tangential component of the load, and the enhancement of the output voltage of the harvester.

3. The piezoelectric harvester was placed behind a cylindrical and an equilateral upstream obstacle. It is found that the cylindrical obstacle is more effective than the equilateral shell in voltage amplification when it is placed at the normalized distance of 5.

4. Since the water wave height depends on the penetration depth of the wavemaker, by increasing the penetration depth in the range of 3 cm to 6 cm, the generated voltage was increased.

5. The effect of the added mass, the form drag, the paddle shape, and the torsional moment on the deformation of the beam and the output voltage has been discussed. It is found that adding the torsional moment resulted in about 13% and 50% increase in the RMS and the peak-to-peak voltages, respectively, with respect to the output of the pure-bending case.

6. The ratio of the RMS voltage and the maximum voltage as a figure of merit for such devices has been computed to be 0.32, 0.30, 0.27, and 0.38 for four piezomaterials using the optical-numerical method.

6 Acknowledgment

This research was supported by the Iran National Science Foundation (Grant number 98017606).

References

[1] Karan, S.K., Maiti, S., Lee, J.H. et al. "Recent advances in self-powered tribo-/piezoelectric energy harvesters: all-in-one package for future smart technologies", Advanced Functional Materials, **30**(48), pp. 2004446 (2020).

https://doi.org/10.1002/adfm.202004446

[2] Ghazanfarian, J., Mohammadi, M.M. and Uchino, K. "Piezoelectric Energy Harvesting: A Systematic Review of Reviews", Actuators, **10**(12), pp. 312 (2021).

https://doi.org/10.3390/act10120312

[3] Kargar, S.M. and Hao, G. "An atlas of piezoelectric energy harvesters in oceanic applications", Sensors, **22**(5), pp. 1949 (2022).

https://doi.org/10.3390/s22051949

[4] Amini, Y., Emdad, H. and Farid, M. "Piezoelectric energy harvesting from vertical piezoelectric beams in the horizontal fluid flows", Scientia Iranica, **24**(5), pp. 2396-2405 (2017).

10.24200/SCI.2017.4240

[5] Cai, W., Roussinova, V. and Stoilov, V. "Piezoelectric wave energy harvester", Renewable Energy, **196**, pp. 973-982 (2022).

https://doi.org/10.1016/j.renene.2022.07.051

[6] Ansari, A., Khavasi, E. and Ghazanfarian, J. "Experimental and SPH studies of reciprocal wet-bed dam-break flow over obstacles", International Journal of Modern Physics C, **32**(7), pp. 2150098 (2021).

https://doi.org/10.1142/S0129183121500984

[7] Xie, X.D., Wang, Q. and Wu, N. "Potential of a piezoelectric energy harvester from sea wave", Journal of Sound and Vibration, **333**(5), pp. 1421-1429 (2014).

https://doi.org/10.1016/j.jsv.2013.11.008

[8] Kargar, S.M. and Guangbo, H. "An Atlas of Piezoelectric Energy Harvesters in Oceanic Applications", Sensors, **22**(5), pp. 1949 (2022).

https://doi.org/10.3390/s22051949

[9] Erturk, A., Inman, D.J. "Piezoelectric energy harvesting", John Wiley & Sons (2011).

10.1002/9781119991151

[10] Xie, X.D., Wang, Q. and Wu, N. "Energy harvesting from transverse ocean waves by a piezoelectric plate", International Journal of Engineering Science, **81**, pp. 41-48 (2014).

https://doi.org/10.1016/j.ijengsci.2014.04.003

[11] Wu, N., Wang, Q. and Xie, X. "Ocean wave energy harvesting with a piezoelectric coupled buoy structure", Applied Ocean Research, **50**, pp. 110-118 (2015).

https://doi.org/10.1016/j.apor.2015.01.004

[12] Oy, S.A. "A design of mass-spring type piezoelectric energy harvesting", Scientia Iranica, **28**(6), pp. 3504-3511 (2021).

10.24200/SCI.2020.54665.3856

[13] Mariello, M., Fachechi, L., Guido, F. et al. "Multifunctional sub-100 μm thickness flexible piezo/triboelectric hybrid water energy harvester based on biocompatible AlN and soft parylene C-PDMS-Ecoflex^{TM}", Nano Energy, **83**, pp. 105811 (2021).

10.1016/j.nanoen.2021.105811

[14] Ghazanfarian, J., Saghatchi, R. and Gorji-Bandpy, M. "SPH simulation of turbulent flow past a high-frequency in-line oscillating cylinder near free-surface", International Journal of Modern Physics C, **27**(12), pp. 1650152 (2016).

https://doi.org/10.1142/S0129183116501527

[15] Dai, H.L., Abdelkefi and A., Wang, L. "Piezoelectric energy harvesting from concurrent vortex-induced vibrations and base excitations", Nonlinear Dynamics, **77**(3), pp. 967-981 (2014).

https://doi.org/10.1007/s11071-014-1355-8

[16] Molino-Minero-Re, E., Carbonell-Ventura, M. and Fisac-Fuentes, C. et al. "Piezoelectric energy harvesting from induced vortex in water flow", *IEEE International Instrumentation and Measurement Technology Conference Proceedings*, pp. 624-627 (2012).

10.1109/I2MTC.2012.6229686

[17] Lee, H.J., Sherrit, S., Tosi, L.P. et al. "Piezoelectric energy harvesting in internal fluid flow", Sensors, **15**(10), pp. 26039-26062 (2015).

https://doi.org/10.3390/s151026039

[18] Bahmanziari, S. and Zamani, A.A. "A new framework of piezoelectric smart tiles based on magnetic plucking, mechanical impact, and mechanical vibration force mechanisms for electrical energy harvesting" Energy Conversion and Management, **299**, pp. 117902 (2024).

10.1016/j.enconman.2023.117902

[19] Burns, J.R., Ocean wave energy conversion using piezoelectric material members, US patent No. 4685296 (1987).

[20] Kazemi, Sh., Nili-Ahmadabadi, M., Tavakoli, M.R. et al. "Energy harvesting from longitudinal and transverse motions of sea waves particles using a new waterproof piezoelectric waves energy harvester", Renewable Energy, **179**, pp. 528-536 (2021).

10.1016/j.renene.2021.07.042

[21] Song, R., Shan, X., Lv, F. et al. "A novel piezoelectric energy harvester using the macro fiber composite cantilever with a bicylinder in water", Applied Sciences, **5**(4), pp. 1942-1954 (2015).

https://doi.org/10.3390/app5041942

[22] Sui, G., Shan, X., Hou, C. et al. "An underwater piezoelectric energy harvester based on magnetic coupling adaptable to low-speed water flow", Mechanical Systems and Signal Processing, **184**, pp. 109729 (2023).

10.1016/j.ymssp.2022.109729

[23] Hassan, M.M., Hossain, M.Y., Mazumder, R. et al. "Vibration energy harvesting in a small channel fluid flow using piezoelectric transducer", *AIP Conference Proceedings* **1754**(1) pp. 050041 (2016).

10.1063/1.4958432

[24] Allen, J., Techet, A., Kelso, R. et al. "Energy harvesting eel", *14th Australasian Fluid Mechanics Conference*, Australia, pp. 685-688 (2001).

https://hdl.handle.net/2440/28722

[25] Mujtaba, A., Latif, U., Oddin, U., et al. "Hydrodynamic energy harvesting analysis of two piezoelectric tandem flags under influence of upstream body's wakes", Applied Energy, **282**, pp. 116173 (2021).

10.1016/j.apenergy.2020.116173

[26] Shan, X., Deng, J., Song, R. et al. "A piezoelectric energy harvester with bending-torsion vibration in low-speed water", Applied Sciences, **7**(2), pp. 116 (2017).

https://doi.org/10.3390/app7020116

[27] Song, R., Shan, X., Lv, F. et al. "A study of vortex-induced energy harvesting from water using PZT piezoelectric cantilever with cylindrical extension", Ceramics International, **41**, pp. 768-773 (2015).

10.1016/j.ceramint.2015.03.262

[28] Latif, U., Younis, M.Y., Idrees, S. et al. "Synergistic analysis of wake effect of two cylinders on energy harvesting characteristics of piezoelectric flag", Renewable and Sustainable Energy Reviews, **173**, pp. 113114 (2023).

10.1016/j.rser.2022.113114

[29] Shan, X., Song, R., Liu, B. et al. "Novel energy harvesting: A macro fiber composite piezoelectric energy harvester in the water vortex", Ceramics International, **41**, pp. 763-767 (2015).

10.1016/j.ceramint.2015.03.219

[30] Karimzadeh, A., Roohi, R. and Akbari, M. "Piezoelectric wind energy harvesting from vortex induced vibrations of an elastic beam", Scientia Iranica, **30**(1), pp. 77-89 (2022).

10.24200/SCI.2022.59718.6393

[31] Hu, S., Zhao, D., Sun, W., et al. "Investigation on galloping piezoelectric energy harvester considering the surface roughness in low velocity water flow", Energy, **262**, pp. 125478 (2023).

10.1016/j.energy.2022.125478

[32] Li, B., You, J.H. and Kim, Y.J. "Low frequency acoustic energy harvesting using PZT piezoelectric plates in a straight tube resonator", Smart Materials and Structures, **22**(5), pp. 055013 (2013).

10.1088/0964-1726/22/5/055013

[33] Zhang, L.B., Abdelkefi, A., Dai, H.L. et al. "Design and experimental analysis of broadband energy harvesting from vortex-induced vibrations", Journal of Sound and Vibration, **408**, pp. 210-219 (2017).

10.1016/j.jsv.2017.07.029

[34] Weinstein, L.A., Cacan, M.R., So, P.M. et al. "Vortex shedding induced energy harvesting from piezoelectric materials in heating, ventilation and air conditioning flows", Smart Materials and Structures, **21**(4), pp. 045003 (2012).

10.1088/0964-1726/21/4/045003

[35] Belkourchia, Y., Bakhti, H. and Azrar, L. "Numerical simulation of FSI model for energy harvesting from ocean waves and beams with piezoelectric material", *6th International Renewable and Sustainable Energy Conference* (2018).

10.1109/IRSEC.2018.8702943

[36] Yamac, H. and Koca, A. "Numerical analysis of wave energy converting systems in case of using piezoelectric materials for energy harvesting", Journal of Marine Engineering & Technology, **20**(2), pp 1-12 (2021).

10.1080/20464177.2018.1529650

[37] Adabzadeh, H, Mohammadi, M.M. and Ghazanfarian, J. "Energy harnessing from water waves by a piezoelectric energy harvester with and without ore-like tip; an experimental study", Amirkabor Journal of Mechanical Engineering, **55**(10), pp. 1195-1206 (2024).

10.22060/MEJ.2023.22347.7604

[38] Khorramdarreh, E.R., Mohammadi, M.M. and Ghazanfarian, J. "A novel floating piezoelectric energy harvesting from water waves: fully-coupled simulation", arXiv preprint arXiv:2306.11901 (2023).

[39] Taylor, J. "Introduction to error analysis, the study of uncertainties in physical measurements, 2nd Edn., University Science Books (1997).

[40] Kundu, S. and Nemade, H.B. "Modeling and simulation of a piezoelectric vibration energy harvester", Procedia Engineering, **144**, pp. 568-575 (2016).

10.1016/j.proeng.2016.05.043

[41] Liu, H., Zhong, J., Lee, C. et al. "A comprehensive review on piezoelectric energy harvesting technology: Materials, mechanisms, and applications", Applied Physics Reviews, **5**(4), pp. 041306 (2018).

https://doi.org/10.1063/1.5074184

Technical biography

Seyyed Behnam Hosseini was MSc student of Mechanical Engineering at University of Zanjan. He is now graduated. His research interests are energy related topics such as energy harvesting and refrigeration systems.

Dr. Mohammad Mostafa Mohammadi is assistant professor of Manufacturing at University of Zanjan where he teaches various courses in graduate and undergraduate levels. His research interests are micro-fabrication, electrochemical manufacturing processes, and piezoelectric transducers and energy harvesters. He obtained his BSc from University of Tabriz, MSc from University of Tarbiat Modares, and PhD from University of Tehran.

Dr. Jafar Ghazanfarian has been an Associate Professor of Mechanical Engineering at University of Zanjan since 2016, and he has taught continuum mechanics for 5 years. Dr. Ghazanfarian has published 42 papers in high-quality WOS-indexed journals, 2 book chapters, and a textbook "Applied Continuum Mechanics for Thermofluids" published by CRC Press. His publications have collected 1167 citations with the h-index of 22 and i10-index of 33 based on the database of GoogleScholar (April 2024). He is the chair of the "Complex Heat and Flow Simulation (CHFS)" research group, which currently works on non-Fourier models, nanoscale heat transport, modern computational fluid dynamics, moving boundary problems, machine learning tools in mechanical engineering, biological thermofluids, aeroacoustics, and renewable energies. He has recorded over 750 hours of free educational videos on different topics of mechanical engineering (in Persian and English). He has also served as referee for a wide range of prestigious journals. Dr. Ghazanfarian is the winner of "Prof. Kazemi Ashtiani's scholarship award" from Iranian national elite's committee, Sentinels of Science Award (medal of excellence in peer review), and top peer reviewer based on Publons' database.

List of Figures

List of Tables

Tab. 1: Physical properties and geometrical details of the setup.

Parameter	Symbol	Unit	Value
Density of the beam	ρ_b	$\frac{kg}{m^3}$	7850
Density of the piezoelectric material	ρ_p	$\frac{kg}{m^3}$	7500
Young's modulus of the Piezomaterial	E_p	GPa	65
Young's modulus of the beam	E_b	GPa	200
Thickness of the piezoelectric layer	h_p	mm	2
Thickness of the beam	h_b	mm	35
Length of the cantilever beam	L	mm	220
Width of the cantilever beam	L	mm	25

Tab. 2: Range of variation of the input parameters of experiments.

	Parameter	Range of variation	Unit
1	The longitudinal distance (L)	40-100	cm
2	the harvester depth (h_1)	2.5, 4.5, 6.5	cm
3	The wave-maker depth (h_2)	3.0, 4.5, 6.0	cm
4	The shape of the oar	Rectangle, triangle, square, trapezoid	-
5	The beam angle	3.0, 4.5, 6.0	degree
6	The shape of the obstacle	Circular and triangular cylinders	-

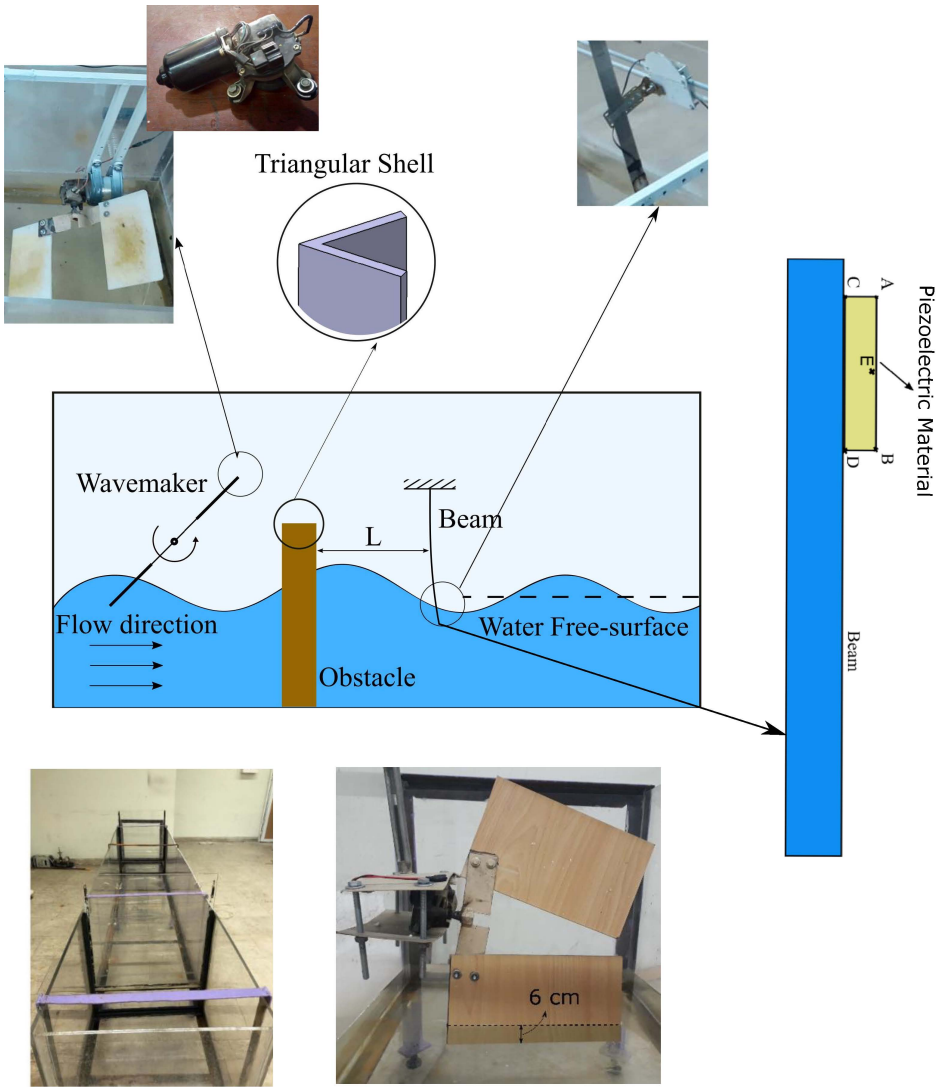

Fig. 1: Schematic representation and geometrical details of the experimental setup, including the wave-maker, the driving motor, the beam, the upstream obstacle, details of attachment of the piezoelectric material to the beam, the water channel, and 6 cm wavemaker indentation.

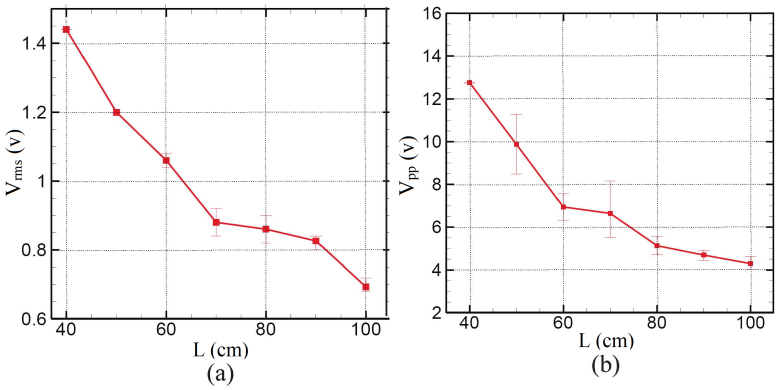

Fig. 2: Variation of (a) the RMS voltage, (b) the peak-to-peak voltage with respect to the longitudinal distance.

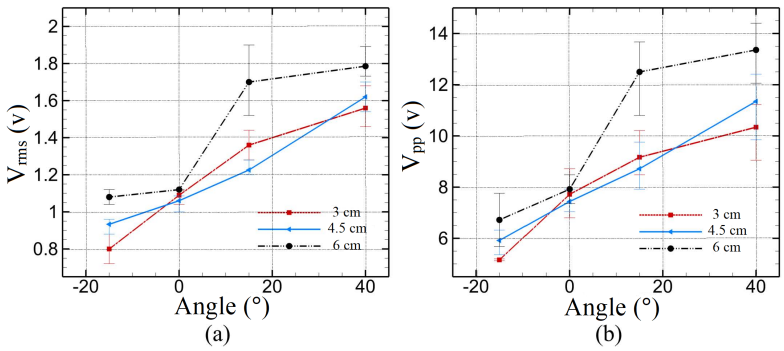

Fig. 3: Variation of the output voltage versus the beam tilt angle for the penetration depths of 3.0 cm, 4.5 cm, 6.0 cm, (a) the RMS voltage, (b) the peak-to-peak voltage.

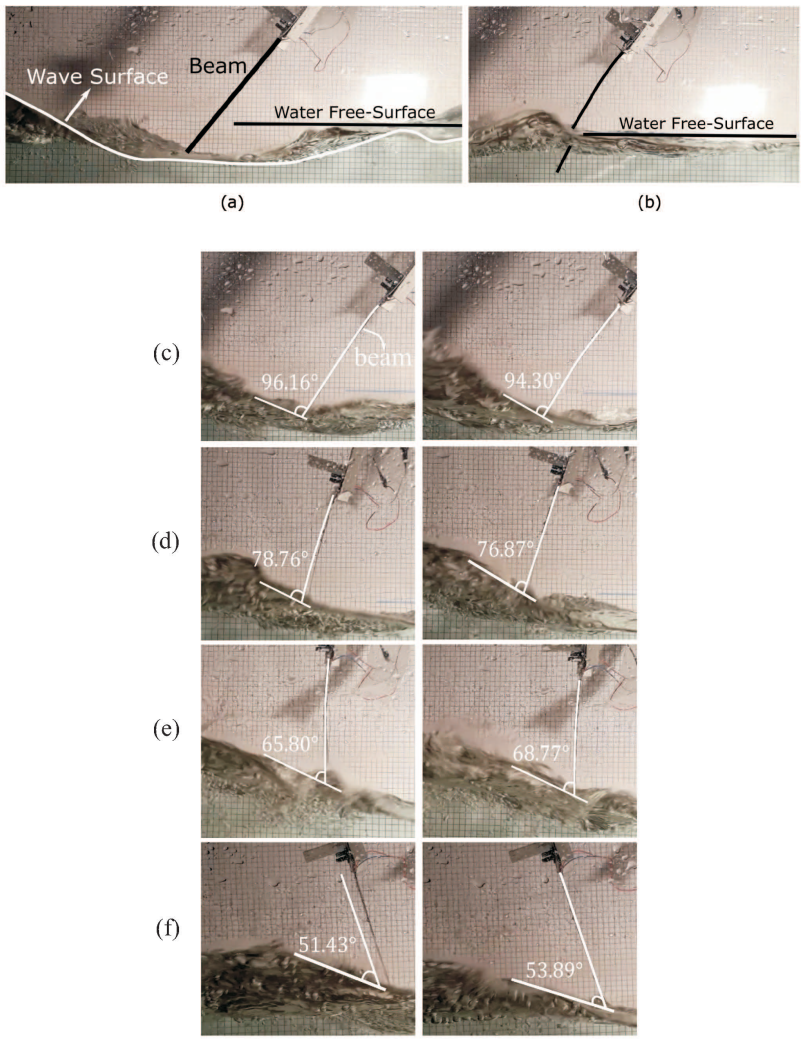

Fig. 4: The flow pattern and the measured contact angle between the beam and the water wave at (a-c) 40°, (d) 15°, (e) 0°, (f) −15° tilt angles.

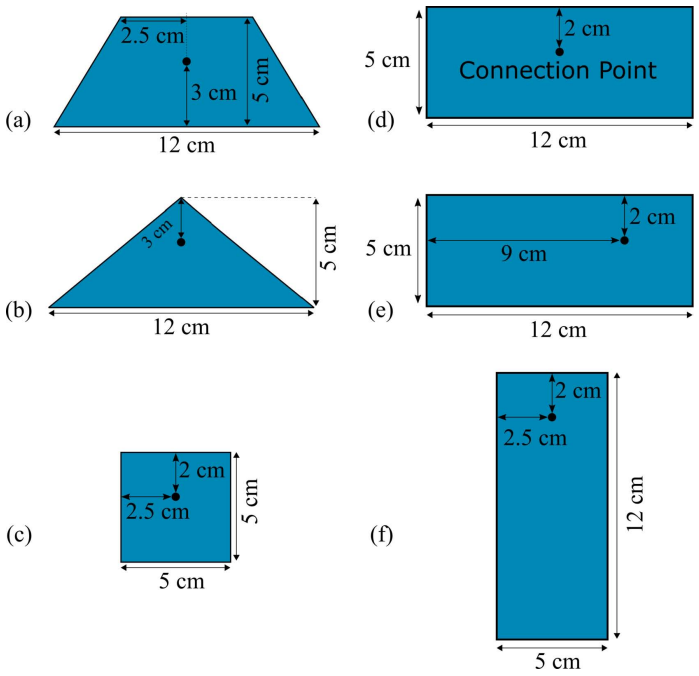

Fig. 5: Different cross sections of the oar-shaped tip of the piezo-beam, (a) trapezoid, (b) triangle, (c) square, (d) concentric horizontal rectangle, (e) eccentric horizontal rectangle, (f) vertical rectangle.

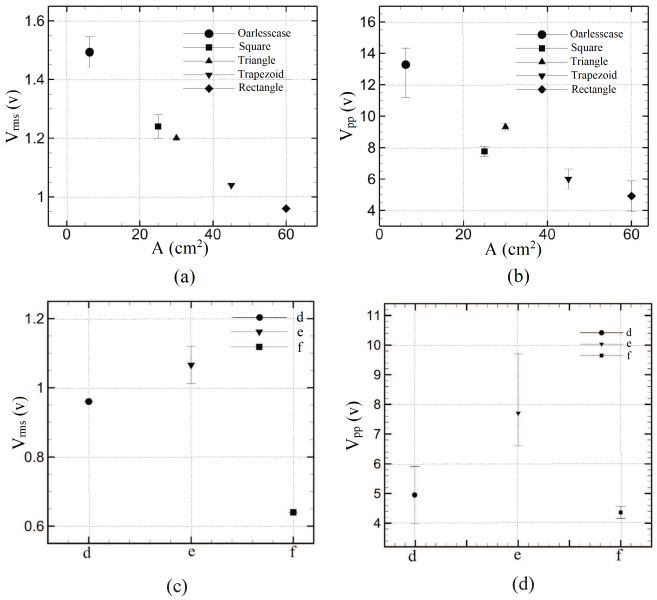

Fig. 6: Variation of (a,c) the output RMS voltage, (b,d) the peak-to-peak voltage for the oarless case as well as the square, triangular, trapezoid, and rectangular oars. The second row corresponds to the data for three rectangular oars labeled d, e, f in Fig. 5.

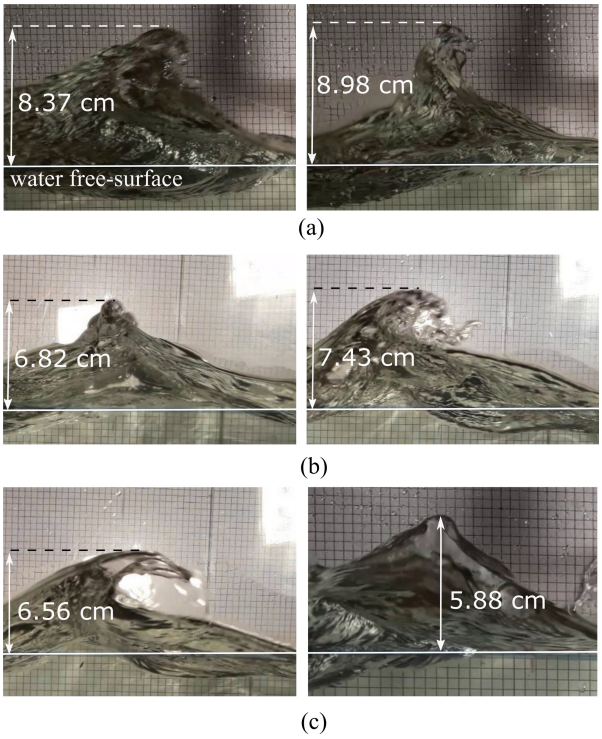

Fig. 7: The measured wave heights for different wave-maker penetration depths, (a) 6 cm penetration depth, (b) 4.5 cm penetration depth, (c) 3 cm penetration depth.

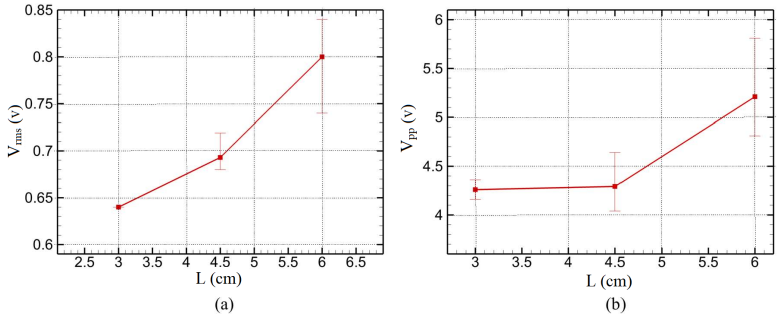

Fig. 8: Variation of the output voltage of the harvester as a function of the penetration depth of the wave-maker, (a) the RMS voltage, (b) the peak-to-peak voltage.

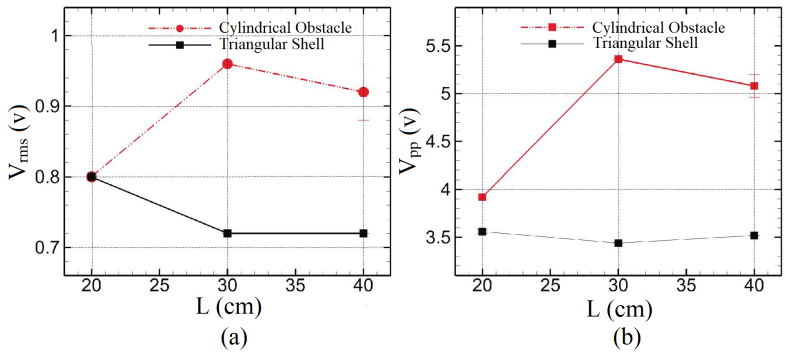

Fig. 9: Variation of the output voltage versus the position of the obstacle, (a) the RMS voltage, (b) the peak-to-peak voltage.

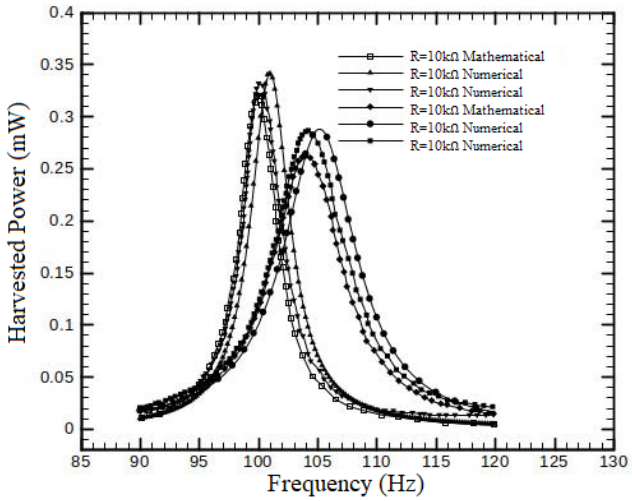

Fig. 10: Variation of the output power at two resistances, analytical and first numerical data from [40] and the second numerical data obtained from the present study.

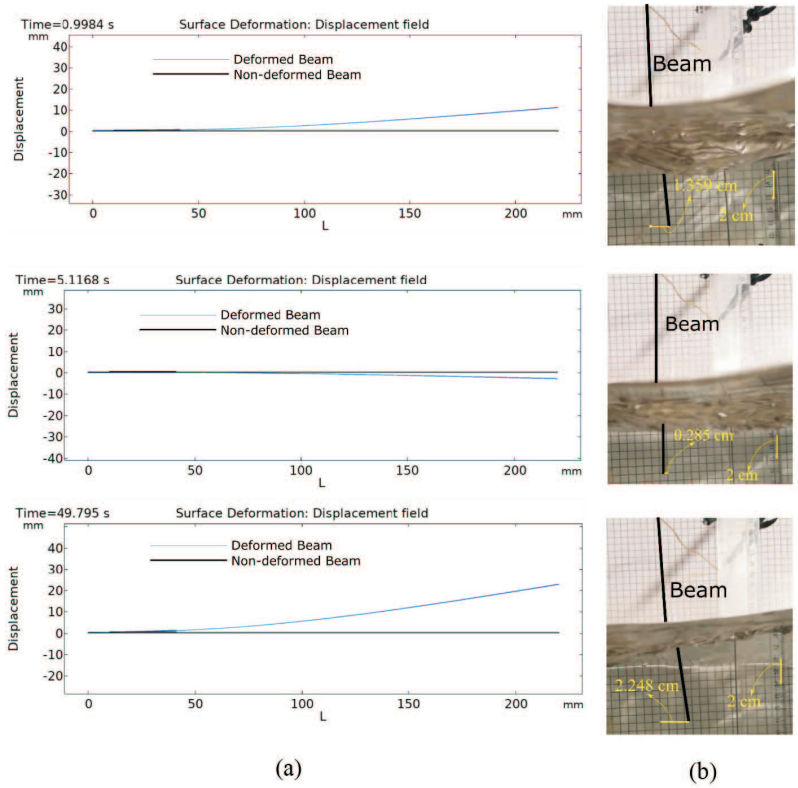

Fig. 11: (a) Simulated deflection of the harvester beam, (b) the visualized deflection at 0.9984 s, 5.1168 s, 49.7950 s.

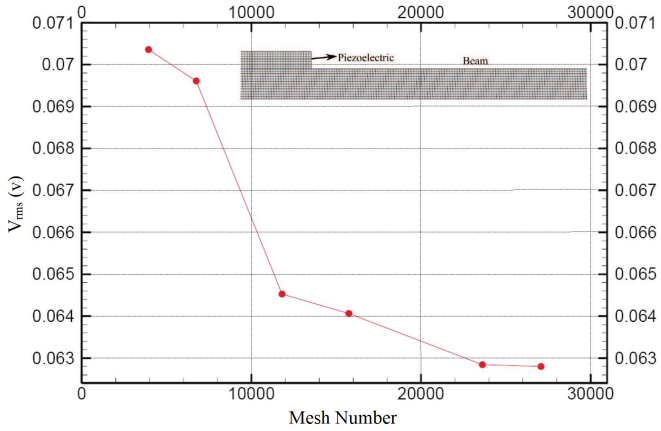

Fig. 12: Results of the mesh-independence study and the RMS voltage as the convergence indicator.

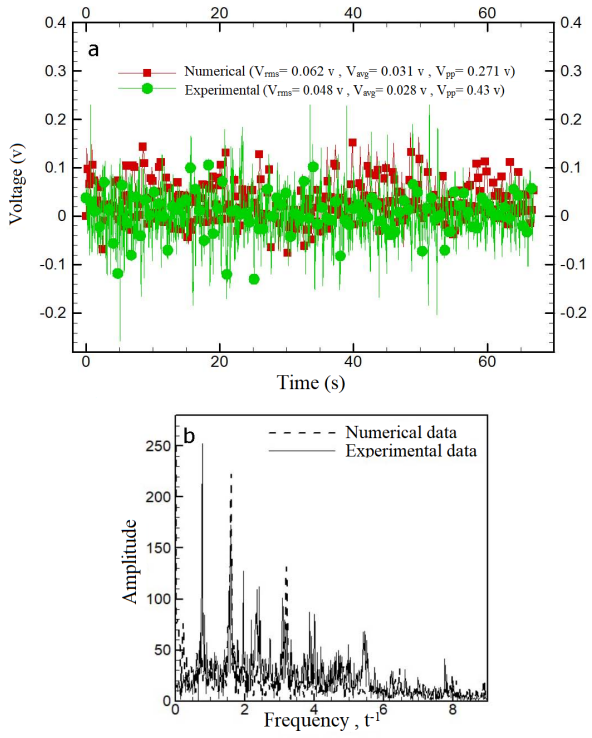

Fig. 13: a) Temporal variation of the measured and the simulated output voltages of the piezoelectric harvester. The RMS, the average, and the peak-to-peak voltages reported in the legend. b) Fourier transform of time histories of the data obtained from experimental and numerical data.

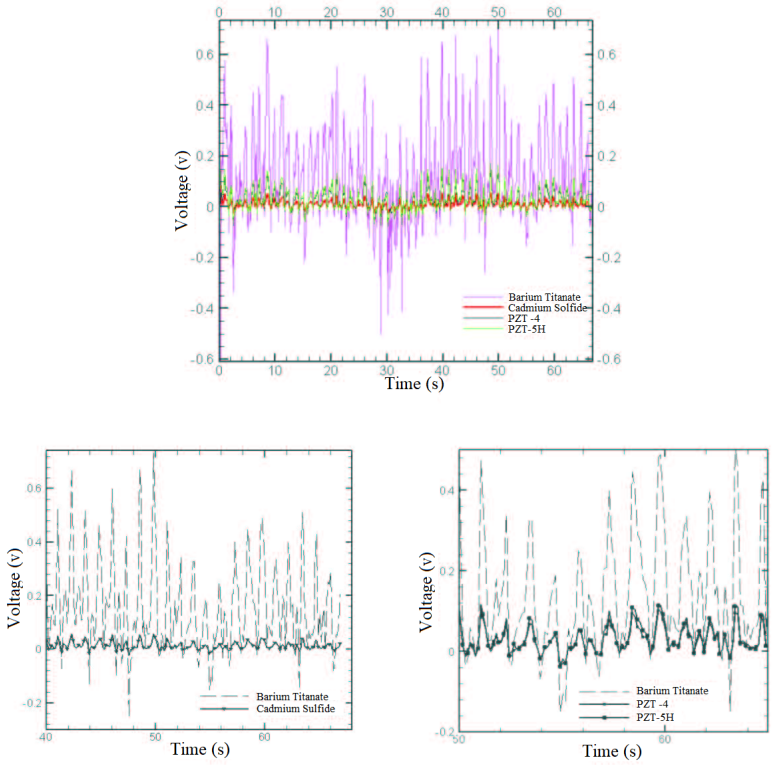

Fig. 14: Comparison of the output voltage obtained from the numerical modeling using five different piezomaterials: barium titanate, cadmium sulfide, PZT-5H, and PZT-4, (a) all cases in one view, (b-c) close snapshots of the output voltage for each case.

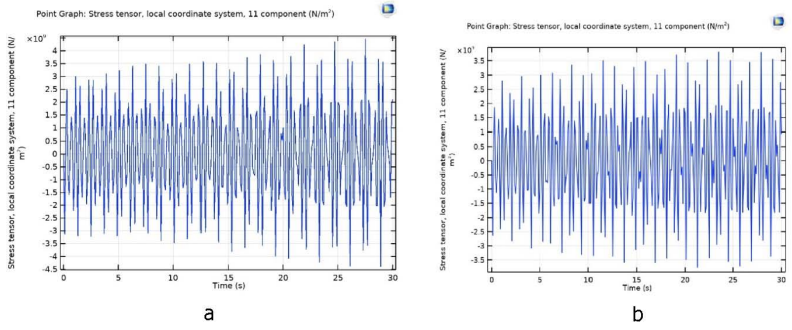

Fig. 15: The stress component T_{11} on: a) barium titanate, b) PZT 5H.